Northern Monterey Bay upwelling shadow front: Observations of a coastally and surface-trapped buoyant plume

C. B. Woodson,[1,2] L. Washburn,[3] J. A. Barth,[4] D. J. Hoover,[5] A. R. Kirincich,[6] M. A. McManus,[2] J. P. Ryan,[7] and J. Tyburczy[8]

[1] During the upwelling season in central California, northwesterly winds along the coast produce a strong upwelling jet that originates at Point Año Nuevo and flows southward across the mouth of Monterey Bay. A convergent front with a mean temperature change of $3.77 \pm 0.29°C$ develops between the warm interior waters and the cold offshore upwelling jet. To examine the forcing mechanisms driving the location and movement of the upwelling shadow front and its effects on biological communities in northern Monterey Bay, oceanographic conditions were monitored using cross-shelf mooring arrays, drifters, and hydrographic surveys along a 20 km stretch of coast extending northwestward from Santa Cruz, California, during the upwelling season of 2007 (May–September). The alongshore location of the upwelling shadow front at the northern edge of the bay was driven by: regional wind forcing, through an alongshore pressure gradient; buoyancy forces due to the temperature change across the front; and local wind forcing (the diurnal sea breeze). The upwelling shadow front behaved as a surface-trapped buoyant current, which is superimposed on a poleward barotropic current, moving up and down the coast up to several kilometers each day. We surmise that the front is advected poleward by a preexisting northward barotropic current of 0.10 m s^{-1} that arises due to an alongshore pressure gradient caused by focused upwelling at Point Año Nuevo. The frontal circulation (onshore surface currents) breaks the typical two-dimensional wind-driven, cross-shelf circulation (offshore surface currents) and introduces another way for water, and the material it contains (e.g., pollutants, larvae), to go across the shelf toward shore.

1. Introduction

[2] Regional-scale winds are believed to be the dominant forcing mechanism for coastal processes within the eastern Pacific upwelling zone also known as the California Current Large Marine Ecosystem (CCLME) [*Hickey*, 1979; *Traganza et al.*, 1987; *Breaker and Broenkow*, 1994]. However, because of a lack of observations, little is known about the relative importance of regional-scale versus local-scale winds in driving currents and altering water properties in nearshore environments within the CCLME. A few studies indicate that local winds and buoyancy gradients are the dominant forcing mechanisms in the nearshore zone [*Graham*, 1993; *Storlazzi et al.*, 2003; *Kirincich et al.*, 2005]. These local processes can alter or even reverse transport of water masses, phytoplankton, larvae, and pollutants expected due to regional forcing [*Shanks and Brink*, 2005]. For example, fronts often develop between recently upwelled waters and warmer nearshore waters in many coastal locations of the CCLME [*Graham*, 1993; *Wing et al.*, 1995]. Such convergent fronts are well known to have increased numbers of phytoplankton, zooplankton, and organisms from higher trophic levels due to passive accumulation and/or organism behavior [*Healey et al.*, 1990; *Franks*, 1995; *Pineda*, 1999; *Woodson and McManus*, 2007; *Ryan et al.*, 2008a, 2008b].

[3] An example of an upwelling convergent front exists at the northern edge of Monterey Bay. Regional-scale upwelling winds create a cold upwelling jet that extends from

[1]Environmental Fluid Mechanics Lab, Stanford University, Stanford, California, USA.
[2]Department of Oceanography, University of Hawai'i at Mānoa, Honolulu, Hawaii, USA.
[3]Geography Department, University of California, Santa Barbara, Santa Barbara, California, USA.
[4]College of Oceanic and Atmospheric Sciences, Oregon State University, Corvallis, Oregon, USA.
[5]United States Geological Survey, Santa Cruz, California, USA.
[6]Woods Holes Oceanographic Institute, Woods Hole, Massachusetts, USA.
[7]Monterey Bay Aquarium Research Institute, Moss Landing, California, USA.
[8]Department of Zoology, Oregon State University, Corvallis, Oregon, USA.
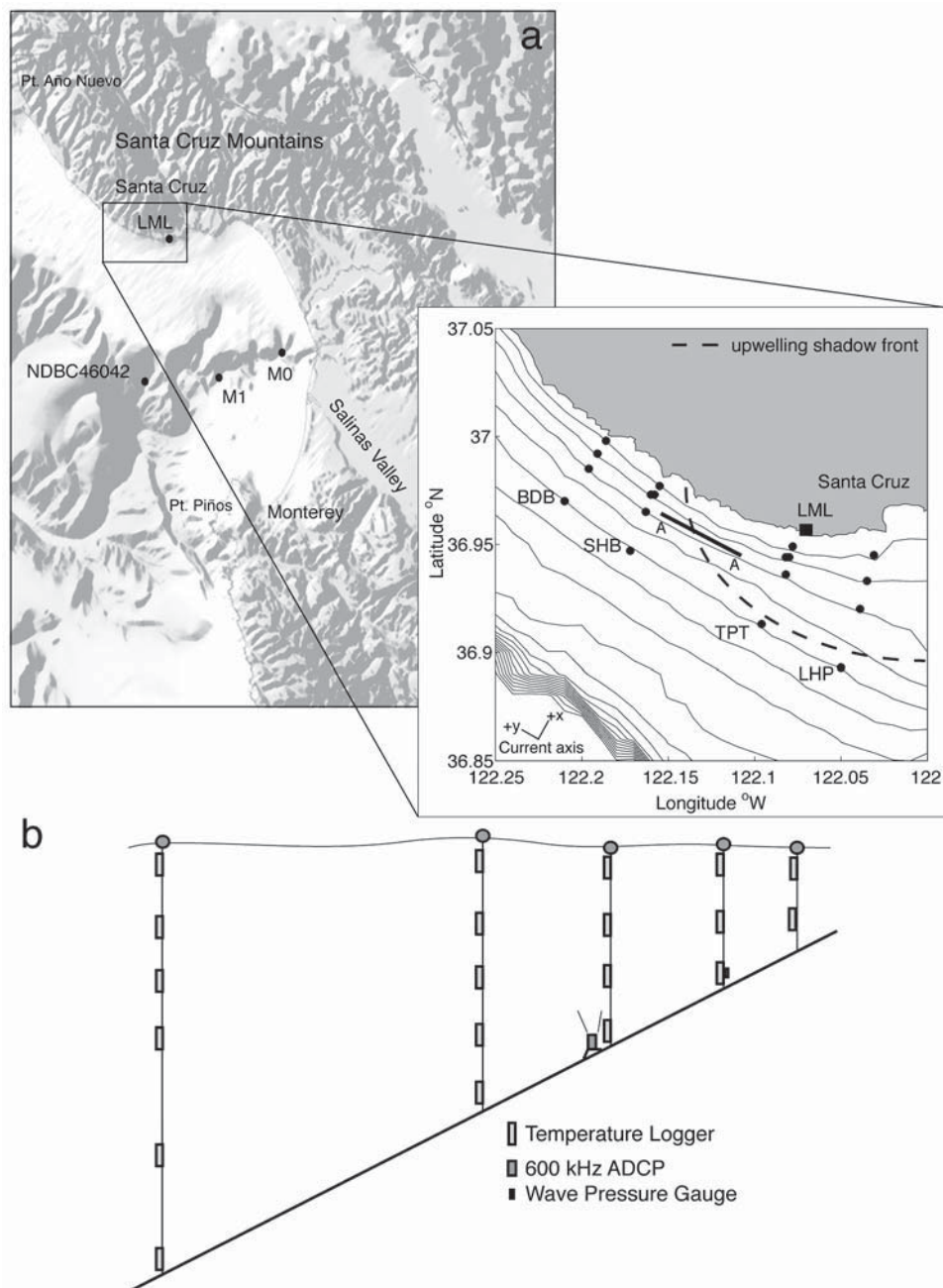
Figure 1. (a) Map of the study site showing mooring array layout; the line "A-A" locates the cross-section in Figure 2. (b) Cross-section of the physical mooring array showing instrumentation and relative depths of both moorings and instruments; representative of all four study sites (not to scale).

Point Año Nuevo southward across the mouth of Monterey Bay (Figure 1a) separating the bay from offshore waters [*Breaker and Broenkow*, 1994; *Rosenfeld et al.*, 1994]. The upwelling flow then either circulates through the Bay or continues southward and joins the Point Sur upwelling jet generated to the south [*Rosenfeld et al.*, 1994]. In the northern bay a retention zone (the "upwelling shadow") develops [*Graham*, 1993; *Graham and Largier*, 1997]. Intense surface heating and reduced wind velocities in the shadow of the Santa Cruz mountains lead to decreased mixing and increased heat gain resulting in increased stratification and the reinforcement of a convergent front at the northern boundary of Monterey Bay [*Graham*, 1993; *Beardsley et al.*, 1998]. Dominant circulation patterns include northwestward alongshore currents within shadow and southeastward currents offshore of the upwelling front [*Graham*, 1993; *Graham and Largier*, 1997]. Temperatures within the upwelling shadow often exceed 15°C in the upper 5 m of the water column but can be 10°C in the lower portion of the water column. These cold temperatures are similar to upwelling plume waters [*Graham and Largier*, 1997; *Woodson et al.*, 2007].

[4] In addition, warming in the Salinas Valley to the southeast produces a strong southeastward atmospheric pressure gradient during midday resulting in intense alongshore winds during the afternoon, which subside in the early evening [*Beardsley et al.*, 1987; *Banta et al.*, 1993]. These winds reverse near-surface currents within the northern bay and along the coast outside the bay on diurnal time scales. For example, local diurnal upwelling caused by the sea breeze can lead to surface temperature fluctuations as high as 2°C–4°C on a 24 h cycle inside the 20 m isobath with the coldest water temperatures observed during midafternoon [*Woodson et al.*, 2007].

[5] To date, the mechanisms controlling the position of the upwelling shadow front along the coast in northern Monterey Bay and the effects of the front on the subtidal and intertidal communities are not well characterized. This study is part of a collaborative effort to examine the influence of the upwelling shadow front on the delivery and settlement of marine larvae in northern Monterey Bay. In this contribution, we examine the relative importance of regional and local mechanisms including buoyancy forces that determine the location of the upwelling shadow front at the northern edge of the bay. Other contributions will assess the importance of the upwelling shadow front on advective processes such as larval transport and settlement within the region.

2. Methods

2.1. Field Observations

[6] The study region at the northern end of Monterey Bay (Figure 1a) encompassed three long-term nearshore monitoring sites maintained by the Partnership for Interdisciplinary Studies of Coastal Oceans (Figure 1a, Sandhill Bluff (SHB), 20 m, and Terrace Point (TPT), 20 m and 60 m moorings). Twenty new moorings organized in four cross-shelf lines augmented the three existing sites. The existing moorings at TPT-20 and SHB-20 consist of a thermistor chain and an acoustic Doppler current profiler (ADCP). TPT-60 consists of a thermistor chain only. New moorings were deployed across each cross-shelf line at 4, 10, 20, 30 and 60 m isobaths (Figure 1b). The four cross-shelf lines were situated so that the two northern or "outer coast" lines, Boony Doon Beach (BDB) and SHB, were typically located outside or very near the upwelling shadow front and the two "southern coast" lines, TPT and Lighthouse Point (LHP), were located predominantly within the upwelling shadow. The dashed line in Figure 1a indicates an average orientation of the frontal boundary of the upwelling shadow. The study region was characterized by a combination of rock and sand substrate with roughly linear (alongshore) depth profiles. Kelp forests are located intermittently along the coast, most often between the 5 m and the 20 m isobaths. There was little or no salinity signature (<0.5%) due to the absence of significant freshwater inputs in the region during the summer. Therefore, we concentrate this analysis on temperature.

[7] The mooring array was designed to resolve the physical processes of frontal movement, currents, surface gravity waves, internal waves, and water mass variability driven by local and regional winds. A primary interest in this study was to understand local diurnal wind-driven

upwelling and its relationship to alongshore-frontal movement. The array produced nearly continuous data sets of current velocity, water column structure from 21 May to 21 September 2007.

[8] The instruments deployed at each mooring site are listed in Table 1. Temperature loggers (Onset Inc.) on each mooring recorded temperature every 2 min (StowAway Tidbits) or every 30 s (XTI). Surface temperature loggers (0 m), which recorded at 4 min intervals, were the only exception. ADCPs (RDI Workhorse 300 or 600 kHz, Teledyne Inc.) were located on each line of moorings lines at the 20 m isobath near each 20 m thermistor mooring. All ADCPs recorded 45 pings per ensemble every 2 min throughout the study period. The shallowest depth bin for water velocity data from the upward looking ADCPs was 2 m. For the remainder of the paper, poleward currents are defined as northwestward (westward), alongshore, and equatorward currents are defined as southeastward (eastward), alongshore. These definitions are adopted due to changes in coastline orientation over the study region.

[9] Offshore and coastal winds were obtained from National Data Buoy Center (NDBC) buoy 46042 and from Long Marine Laboratory, respectively (LML) (Figure 1a). Satellite images of sea surface temperature (SST) in the Monterey Bay region from the Moderate Resolution Imaging Spectroradiometer (MODIS) sensor were obtained 12 times during the experiment. Image processing methods are detailed by *Ryan et al.* [2008b]. Surface drifters (drogue depth 1–2 m) were released at two separate intervals as part of a concurrent study in the region: one during a wind relaxation (10–13 July 2007) and one during upwelling conditions (20–24 July 2007). Deployments were typically for 3–4 days. Further analysis of drifter tracks will be reported in a separate contribution.

[10] In addition, during an intensive sampling period in July, conductivity-temperature-depth (CTD) casts were made at each mooring site and at stations across the upwelling shadow front. These surveys occurred on 11, 13, 15, 16, 21, 24, and 27 July 2007. CTD measurements were also made from a towed undulating vehicle (Acrobat, SeaSciences Inc.). Tows were conducted in a cross-shore direction, along each of the mooring lines and alongshore spanning the study region.

2.2. Frontal Movement Analysis

[11] Diurnal and semidiurnal tides were removed from ADCP data using T_TIDE [*Pawlowicz et al.*, 2002]. Although some of the sea breeze–driven variability may be taken by the S1 tidal component, this component was small relative to the K1 and M2 signals. Also, removal of S1 insures that our estimates of diurnal variability are conservative. Time series of currents were filtered using a low-pass filter with a 40 h half-power period for regional wind-forcing analyses [*Mooers*, 1968]. The frontal propagation speed, c_{obs}, between mooring pairs along the 20 m isobath was estimated as

$$c_{obs} = L/\Delta t_f, \qquad (1)$$

where L was the alongshore distance between the moorings, and Δt_f was the difference in arrival times between the

Table 1. Mooring Locations, Instrument Types, and Depths for Deployments

Mooring Identification	Water Depth (m)	Latitude (°N)	Longitude (°W)	Thermistor Depths (m)	ADCP Range (m)	Major Axis ($y-$)[a] (deg)
Bonny Doon Beach						
BDB002	10	36.998	122.187	0, 5, 9	-	
BDB003	20	36.996	122.194	0, 5, 10, 19	3−17	330
BDB004	30	36.993	122.202	0, 5, 10, 20, 29	-	
BDB005	60	36.975	122.222	0, 5, 10, 20, 40, 59	-	
Sand Hill Bluff						
SHB001[b]	20	36.973	122.160	0, 5, 10, 19	3−17	329
SHB004	10	36.976	122.155	0, 5, 9	-	
SHB005	20	36.973	122.160	0, 5, 10, 19	-	
SHB006	30	36.967	122.156	0, 5, 10, 20, 29	-	
SHB007	60	36.952	122.181	0, 5, 10, 20, 40, 59	-	
Terrace Point						
TPT001[b]	20	36.944	122.085	0, 5, 10, 19	3−15	294
TPT014	10	36.949	122.080	0, 5, 9	-	
TPT015	20	36.944	122.082	0, 5, 10, 19	-	
TPT016	30	36.940	122.085	0, 5, 10, 20, 29	-	
TPT007[b]	60	36.913	122.096	0, 5, 10, 20, 40, 59	-	
Lighthouse Point						
LHP002	10	36.953	122.031	0, 5, 9	-	
LHP003	20	36.947	122.033	0, 5, 10, 19	3−17	276
LHP004	30	36.934	122.034	0, 5, 10, 20, 29	-	
LHP005	60	36.928	122.049	0, 5, 10, 20, 40, 59	-	

[a]Major axis is reported for the depth averaged flow.
[b]Long-term moorings with data sets from 1999 to 2007.

moorings. The width of the front was estimated at each site as

$$\Delta y_f = c_{\text{obs}} \Delta t_c, \qquad (2)$$

where Δt_c was the time required for the temperature at a site to rise or fall to values associated with the upwelling shadow front or the ambient water. These values were taken where the temperature gradient approached 0 ($\mathrm{d}T/\mathrm{d}t < 0.001°C\ s^{-1}$). The times of frontal arrivals at the 20 m moorings was also used to calculate composite averages of currents and temperatures before, during, and after front arrival at SHB and BDB.

[12] The location of the front was determined using two criteria. On the basis of observations of consistent temperatures of near 10°C in upwelling plume waters, we did the following. (1) We used the 11°C isotherm location at 5 m depth as a proxy for the front location along the 20 m isobath. We used an alongshore linear interpolation of the 5 m depth temperature data then added the local internal Rossby radius computed from the hourly averaged temperature profile at the site closest to the front location in order to account for curvature of the pycnocline to the surface. (2) We also used periods that showed reversals in the low-pass filtered, depth-averaged, alongshore flow direction. The time series of front location was smoothed using a low-pass filter with a 6 h half-power period [Mooers, 1968].

2.3. Analyses

[13] Figure 2 provides a schematic of the alongshore frontal cross section, for a two-layer flow in a reference frame moving with the front. Along northern Monterey Bay, movement of the upwelling shadow front is determined by a force balance among an alongshore barotropic pressure difference, baroclinic pressure gradients arising from den-

sity differences, bottom shear stress (τ_b) when the upwelling shadow contacts the seafloor and the wind stress (τ_W). For the two-layer system in Figure 2, τ_b is negligible under most conditions except during strong downwelling favorable winds [Lentz and Largier, 2006]. In addition, interfacial stress due to shearing between the warm surface layer and cooler lower layer may also be important at times. Taking z equal to the depth of the buoyant layer, H, the layer-integrated, alongshore momentum equation becomes

$$V_t + UV_x + VV_y + fU = -(gH^2/2\rho_o)\rho_y - g(H + \eta)\eta_y + \tau_W^y/\rho_o, \qquad (3)$$

where (U, V) are the cross-shore and alongshore depth averaged velocities, respectively, subscript denotes differentiation along (x, y, t), f is the Coriolis parameter, g is the gravitational acceleration, and ρ is the fluid density. Here $g(H + \eta)\eta_y$ is the barotropic pressure gradient and can be estimated from the hydrostatic pressure equation. Also (ρ_y, η_y) are the alongshore density and sea surface anomaly, respectively, and can be evaluated as $(\Delta\rho, \eta)/\Delta y_f$ where Δy_f is the distance across the front. The coordinate system in this formulation is positive x as onshore, cross-shelf and positive y as poleward.

[14] Here $(gH^2/\rho_o)\rho_y$ is the baroclinic pressure gradient resulting from the temperature difference across the front. The wind stress, τ_W, can be estimated using the method of Large and Pond [1981]. As shown by Drake et al. [2005], all terms on the left side of equation (3) are 1 to 2 orders of magnitude less than terms on the right hand side and can therefore be neglected. Also, the alongshore momentum balance at diurnal time scales is not in geostrophic balance
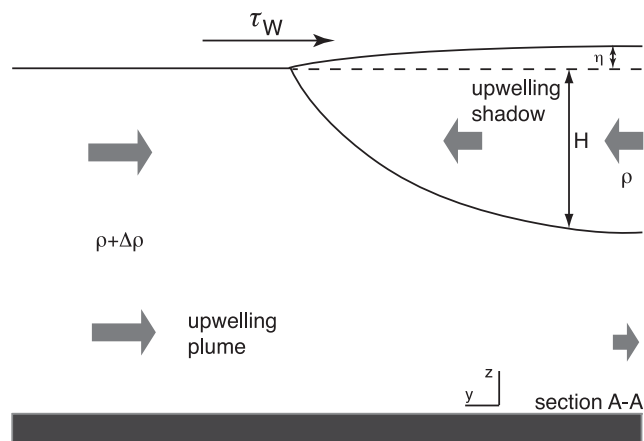
Figure 2. Cross-section view of a convergent, buoyant front, showing analytical parameters and general circulation patterns in a frame of reference moving with the front. H is the depth of the buoyant layer; ρ is the fluid density; η is the sea surface displacement due to buoyant effects; and τ_W is the wind stress.

and Coriolis effects are 2 orders of magnitude less than stress and pressure components [*Drake et al.*, 2005]. The important balance in this case is between the wind stress and the components of the pressure gradient

$$(gH^2/2\rho_o)\rho_y + g(H + \eta)\eta_y = \tau_W^y/\rho_o. \qquad (4)$$

[15] Focused upwelling around Point Año Nuevo decreases sea level while strong solar insolation and warming within the upwelling shadow result in raised sea level within the bay. By substituting known seasonal values of η_y due to regional-scale upwelling for η_x (since $\eta_x \approx \eta_y$ and is largely controlled by upwelling center at Point Año Nuevo), and taking $H \gg \eta$ in the cross-shore momentum equation, the barotropic, alongshore current can be calculated from geostrophy ($V = -g\eta_x/f$), yielding a northward mean flow on the order of 0.10 m s^{-1} [e.g., *Drake et al.*, 2005].

3. Results

[16] During the study, wind conditions were consistent with the upwelling season for central California (Figure 3). Offshore winds at NDBC buoy 46042 were typically from the north-northwest with speeds between 10 and 15 m s^{-1} (Figure 3a). Eleven relaxation events, when winds decreased below 3 m s^{-1} or reversed to originate from the south-southeast, occurred during the study. Consistent with previous observations, local diurnal sea breezes were oriented alongshore equatorward and often reached up to 15 m s^{-1} during the afternoon (Figure 3c) [*Beardsley et al.*, 1987; *Banta et al.*, 1993; *Rosenfeld et al.*, 1994; *Woodson et al.*, 2007].

[17] During relaxation events, the upwelling shadow water mass moved poleward along the coast as evidenced by drifter tracks and SST during relaxation event 5 (Figure 4a). This response was consistent for all wind relaxations during the 2007 upwelling season on the basis of satellite SST images with longer events flushing the entire bay (e.g., event 5, Figure 4a). The offshore upwelling front was not observed to reach the coast during any relaxation period (e.g., Figure 4). Surface temperatures during upwelling-favorable wind periods were on average 2−5°C (∼8−12 to ∼12−17°C) warmer within upwelling shadow than in recently upwelled plume waters offshore (e.g., Figure 4b). Drifters released in the northern bay (inside the upwelling shadow) moved alongshore poleward until reaching the upwelling shadow front and then were entrained into the equatorward directed upwelling jet under
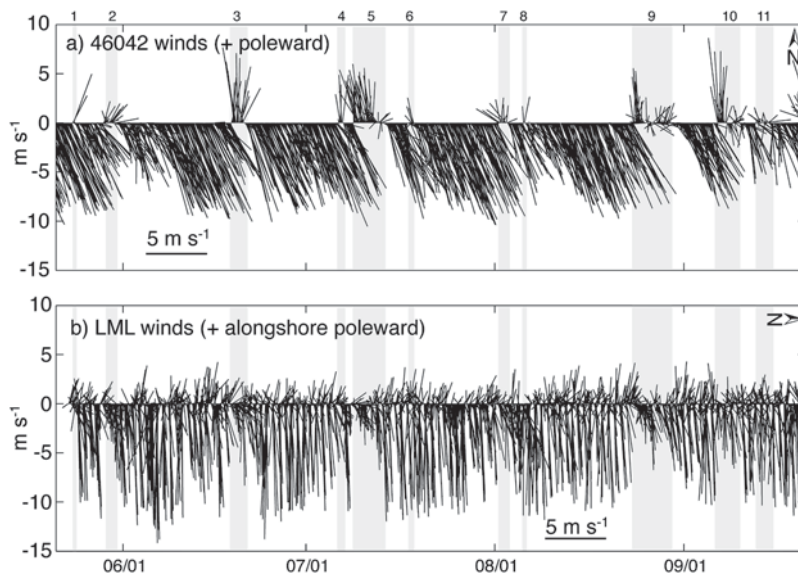
Figure 3. Time series during the study period of (a) regional winds from NOAA NDBC buoy 46042 located ∼20 km off coast in center of Monterey Bay, positive to the north, and (b) alongshore wind speed from Long Marine Laboratory, positive to the east (upwelling favorable). Regional relaxation events are highlighted in gray and numbered above Figure 3a for reference.
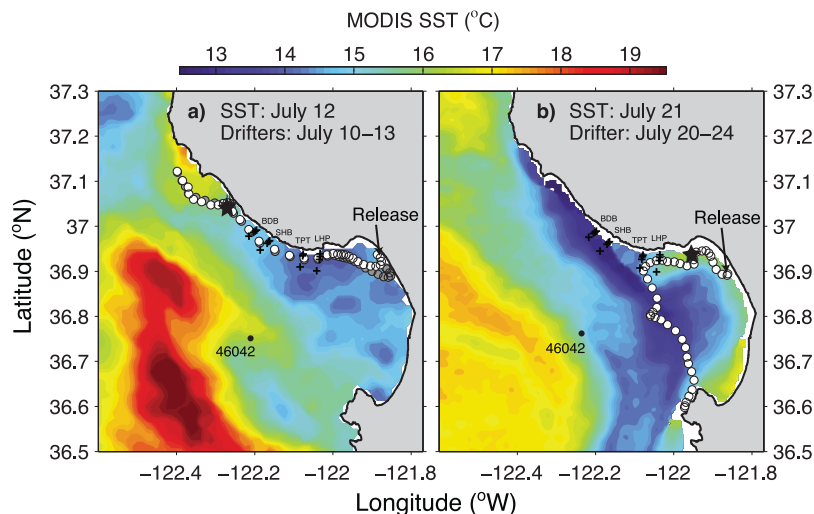
Figure 4. Sea surface temperatures (MODIS) and drifter tracks during (a) relaxation and (b) upwelling. Plus indicates mooring locations for current study. Star indicates location of drifters on date of satellite image shown. Locations (circles) are regularly spaced in time in order to provide relative speeds.

upwelling favorable conditions (Figure 4b). The upwelling shadow was also characterized by higher surface chlorophyll concentrations than upwelling filament waters, consistent with phytoplankton growth resulting from transport of nutrient-rich waters into the bay [*Pennington and Chavez*, 2000]. Transects taken with the Acrobat illustrate the differences in surface layer temperatures between upwelled waters (Figure 5a) and the upwelling shadow plume (Figure 5b). These cross sections suggest the upwelling shadow water mass acts as a two layer flow as described previously because front contact with the bottom occurs within 0.20 km of the coast.

[18] During the prolonged wind relaxation event between 8 and 13 July 2007 (Figure 3, events 4 and 5) upwelling

shadow waters moved poleward along the coast, as suggested by the warm water mass at the end of the drifter track of Figure 4a. During this and the previous relaxation event, temperatures at the BDB and SHB warmed as the upwelling shadow moved up the coast during 6–7 and 8–9 July (Figure 6). Temperatures in Figure 6 have been low-pass filtered (24 h cutoff period) to reduce effects of diurnal temperature fluctuations and make the response to regional winds more apparent. Here regional winds were represented by offshore winds at NDBC buoy 46042. Surface currents on the 20 m isobath on the 4 mooring lines respond to wind relaxations 4 and 5 within a few hours by switching from equatorward to poleward (Figure 7). The northward advection of the upwelling shadow during relaxations 4 and 5 is
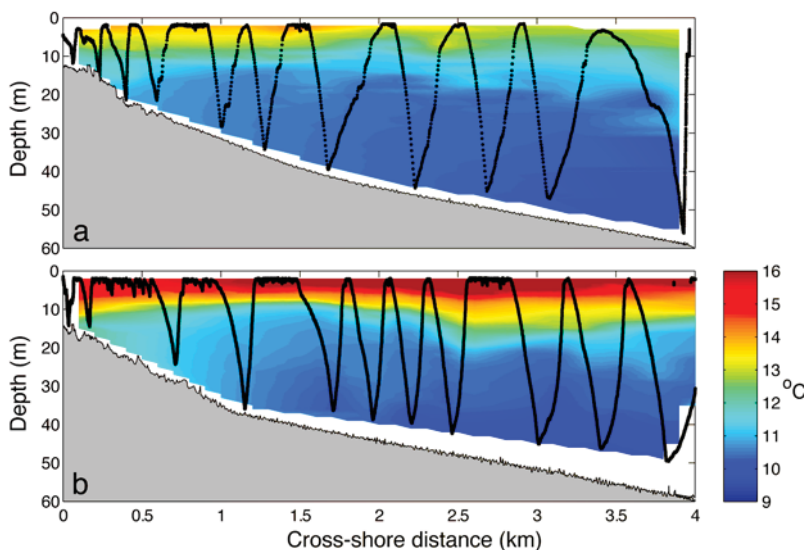
Figure 5. High-resolution across-shelf sections of temperature collected from the Acrobat towed body along the TPT line (a) within the upwelling plume (11 July 2007) and (b) within the upwelling shadow (24 July 2007). The actual track line of the vehicle is shown in thick black while bathymetry collected by the ship's echo sounder is shaded in gray.
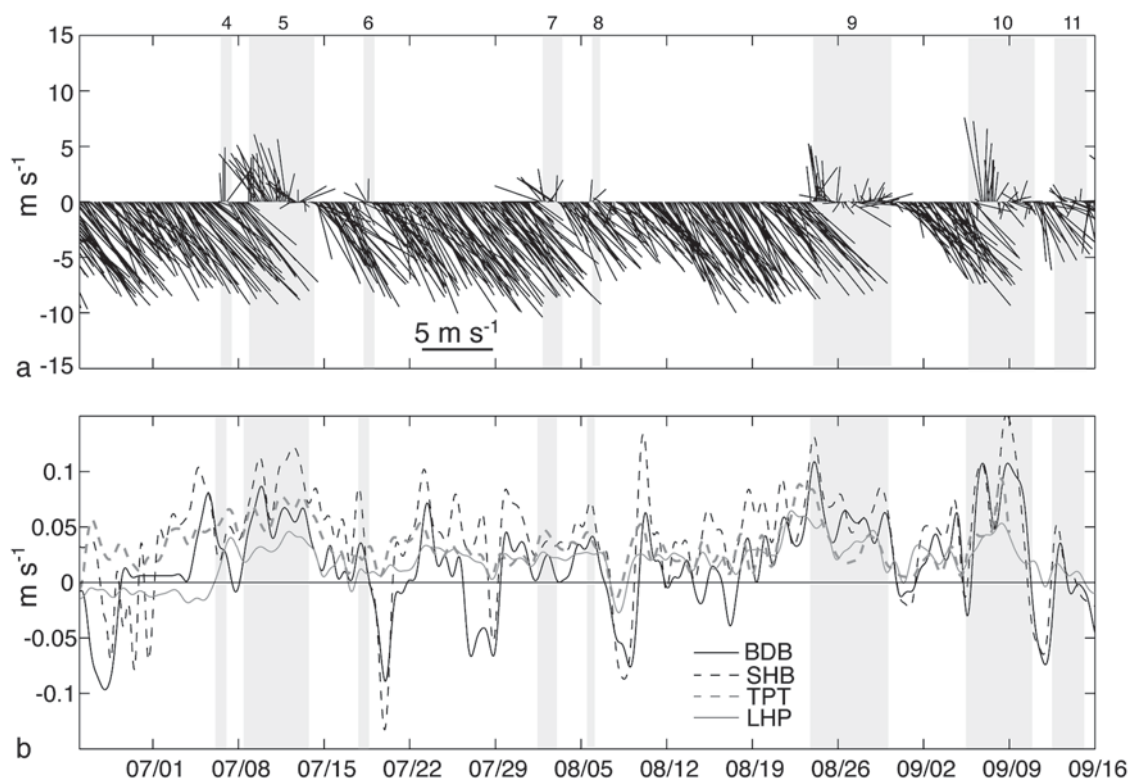
Figure 6. (a) Regional along-shelf winds from NDBC 46042, (b) surface temperature from the 20 m mooring from 2 to 22 July. A 24 h low-pass filter was employed to smooth the temperature time series in Figure 6b. Grey bars denote wind reversals (relaxation events) in Figures 6a and 6b.

indicated by warming at SHB and BDB within a few hours of the wind relaxation (Figures 6b and 7d).

[19] Warming of the water column at TPT and LHP did not occur until several days after the transition back to upwelling favorable winds on 13 July (Figure 6). Observations of increased surface temperature due to cross-shore advection of the offshore, regional upwelling front to the nearshore did not occur even during the longest regional relaxation events (5 days, 5 and 9) at all sites.

[20] The nine shorter relaxation events during the study (events 1−4, 6−8, and 10 and 11) showed similar patterns of cooling at the southern sites (Figure 7). During these events, warm upwelling shadow waters traveled up the coast but were not completely flushed from the bay. It appeared as though warm upwelling shadow waters were advected back into the upper bay after the return to upwelling favorable conditions (satellite and mooring observations). This assertion is further supported because of two reasons. (1) If upwelling moved the tongue offshore, surface waters would cool. However, surface waters warmed in the northern bay faster than possible due to solar heating. (2) If the warm waters simply mixed with the jet, stratification would be minimal; however, stratification increased rapidly, again faster than can be accounted for by solar heating. Shorter relaxation events (<5 days) did not allow sufficient time for the upwelling shadow to move poleward past Point Año Nuevo. Thus, when upwelling favorable conditions resumed, the southward upwelling jet forced the warm water mass back into the bay.

[21] Depth-averaged subtidal currents generally were oriented poleward within the upwelling shadow during the study period consistent with previous observations [*Storlazzi et al.*, 2003; *Drake et al.*, 2005; *Woodson et al.*, 2007]. Northwest of the upwelling shadow, at BDB and SHB, surface currents within the upwelling plume were equatorward (Table 2, Figure 7). The BDB line was typically northwest of the front and consequently experienced an equatorward depth-averaged residual current around 0.02 m s^{-1}. The BDB and SHB lines experienced regular front crossings indicating the front was often located in the vicinity of these moorings. The outer moorings of the LHP line often observed cross-shore front crossings that did not reach shore. In the upper water column (above the thermocline), sites behind or just ahead of the upwelling shadow front experienced poleward mean currents with speeds increasing as the front approached. Below the upwelling shadow water mass (i.e., below the thermocline at $5-10$ m depth), mean current speeds were significantly reduced ($\sim 0.02-0.06$ m s^{-1}) but still were generally oriented poleward.

[22] During upwelling favorable conditions, the BDB line and SHB line were used to calculate frontal depth, h_p, and width, Δy_f. Here h_p was calculated from interpolations of the temperature gradient at the 20 m moorings at sites BDB and SHB. Results were then averaged yielding $h_p = 4.2$ m (Table 3). Visual siting of the front (e.g., Figure 8) during the intensive sampling period suggested that Δy_f was often less than a few meters and could not be resolved by our temporal sampling of $2-4$ min. Interpolations to the mea-
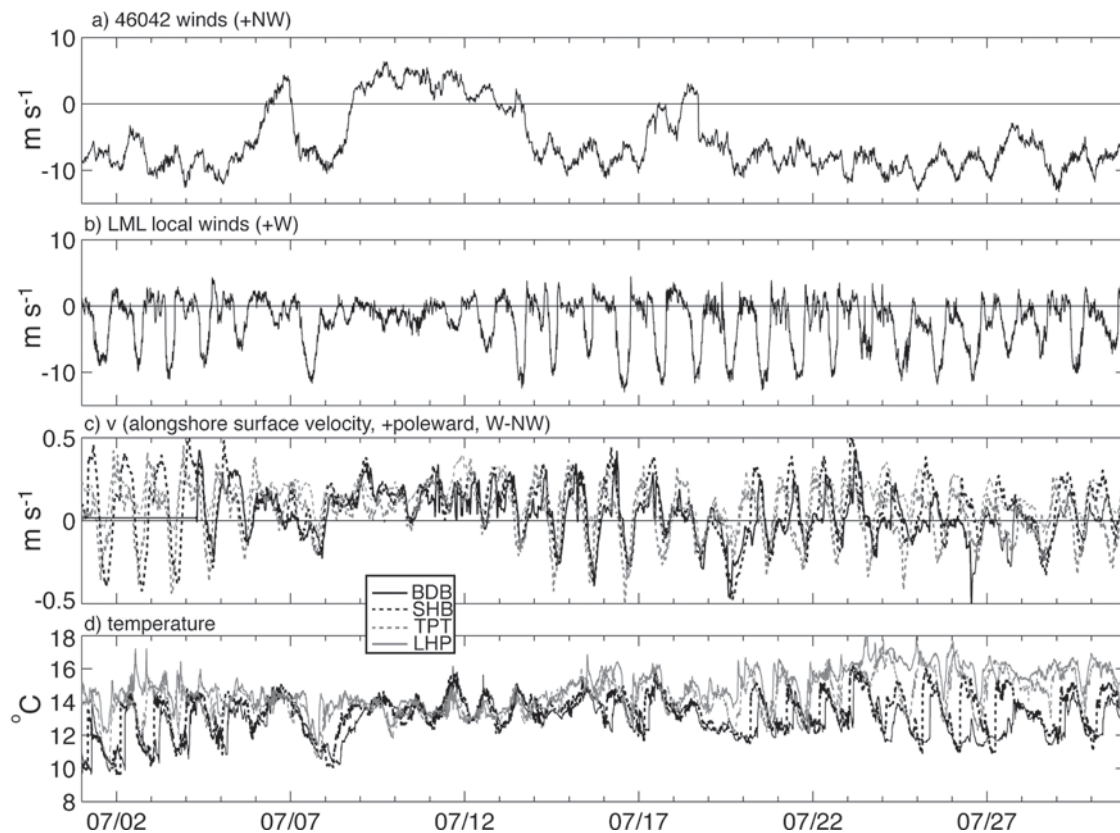
Figure 7. Time series across all sites during July showing (a) alongshore wind speed from NDBC 46042 (positive northwestward), (b) alongshore wind speed at LML (positive poleward), (c) alongshore, depth-averaged current velocities from 20 m mooring ADCPs at each mooring array (positive poleward), and (d) surface temperature at 20 m moorings from each mooring array.

sured temperature data, where possible, yielded estimates of $c_{obs} = 0.3$ m s^{-1} and thus $\Delta y_{f\,min} \sim 70$ m, which is the limit of our spatial resolution with the current observational design. The mean temperature change across the front and the thermocline within the upwelling shadow was $\Delta T_f = 3.77°C \pm 0.29°C$.

[23] The composite averages for 37 frontal crossings at SHB, the most crossings over any of the moorings, are shown in Figure 9. Surface temperature and water column stratification increased sharply as the fronts passed SHB (Figure 9b): surface temperatures rapidly increased by more than 2°C with most of the change occurring within several minutes of frontal passage. The alongshore near-surface velocity also increased abruptly during frontal passage (Figure 9c). At middepth ($\sim$10 m), alongshore currents decreased slightly, and near the bottom ($\sim$18 m) they decreased further. The pattern of alongshore current velocities with depth is consistent with convergence near the surface behind the front, downwelling at the front, and flow away from the front near the bottom. This pattern is superimposed on a diurnal variation in alongshore flow at all depths associated with local diurnal wind variations as described by *Woodson et al.* [2007]. As equatorward winds strengthened during morning hours, poleward near-surface velocities were similar to those at 10 m depth. Later, after alongshore currents at all depths became equatorward, near-

Table 2. Current Profile Characteristics From Four ADCPs Located at Each 20 m Mooring Across Site[a]

Site	Mean Alongshore Velocity (m s^{-1})	Percent of Time Current Oriented Up Coast	Number of Times Front Crossed Site Alongshore	Number of Times Front Crossed Site Cross Shelf
BDB	−0.0232 (11.21)	35.5%	37	0
SHB	0.0466 (13.61)	70.7%	43	0
TPT	0.0715 (13.06)	90.7%	6	0
LHP	0.0138 (9.31)	60.5%	0	25

[a]Mean (and standard deviation) depth-averaged alongshore velocity following a 40 h low-pass filter to remove tidal constituents. Percent of time currents were traveling up coast (northward and westward) shows roughly the fraction of time each site was located within the upwelling shadow. The LHP 20 m site was often located at the outer edge of the upwelling shadow front. At this site, the front often crossed the site in the cross-shelf direction.

Table 3. Comparison of Buoyancy Current Scaling Parameters Using Observational Data During Periods of Light or No Winds[a]

Term and Equation	Definition	Mean ± Standard Deviation	Observed Range
h_p	Thickness of gravity current	4.2 ± 0.2 m	$3.5-4.5$ m
$c_w = \sqrt{g'h_p}$	Propagation speed in limit of steep bottom slope	0.16 ± 0.03 m s^{-1}	$0.07-0.22$ m s^{-1}
$c_\alpha = \alpha g'/f$	Propagation speed in slope-controlled limit	1.77 ± 0.28 m s^{-1}	$0.19-1.59$ m s^{-1}
c_w/c_α	Ratio of propagation speeds <1 surface trapped	0.18 ± 0.04	$0.14-0.35$
$t_{\text{adj}} = 2c_w/fc_\alpha$	Adjustment time scale for foot of front to reach equilibrium	0.86 ± 0.13 h	$0.57-1.04$ h

[a]Periods of light or no winds are specified as <2 m s^{-1}. Values for other parameters not calculated directly from temperature profiles were bottom slope, $\alpha = 0.012$ m m^{-1}, and Coriolis frequency, $f = 0.875'10^{-4}$ s^{-1} (19.9 h inertial period at 37°N).

surface currents were faster than deep currents, which increased shear in the water column.

[24] The pattern of cross-shore flow is also distinctive. Onshore flow occurred near the surface, offshore flow at middepth, and stronger offshore flow near the bottom. These currents are superimposed on a typical upwelling cross-shore current pattern with offshore flow near the surface, weak flow at middepth, and onshore flow near the bottom. This typically upwelling current pattern is interrupted by the flow pattern associated with frontal passages.

[25] Estimates of frontal propagation speeds, c_{obs}, are consistent with forcing by buoyancy differences between the upwelling shadow and recently upwelled waters. To estimate c_{obs} in the absence of local wind effects, frontal propagation between SHB and BDB was examined during early morning hours when winds had been calm for 8 h or more, this occurred commonly prior to frontal arrivals at SHB (Figure 10a). Propagation speed, c_{obs}, was significantly related to temperature differences, ΔT_f, during frontal passages at SHB (black dots, Figure 10a, $R^2 = 0.36$, $N = 37$, $p < 0.001$). After removing tidal currents, the fit between c_{obs} and ΔT_f improved (gray dots, Figure 10a, $R^2 = 0.49$, $N = 37$, $p < 0.001$). Extension of the linear least square fit of ΔT_f versus c_{obs} suggests a mean current of +0.10 m s^{-1} (i.e., poleward) when $\Delta T_f =$

0°C. This offset is consistent with poleward current speeds over $2-4$ h prior to frontal arrivals at SHB as shown in the composite averages of Figure 9c. It also agrees with typical depth-averaged poleward current speeds in the study region reported by *Drake et al.* [2005].

[26] We can further estimate the observed propagation speed as

$$c_{\text{obs}} = c + u_a, \qquad (5)$$

where u_a is the ambient current speed and is estimated for individual frontal passages from near-surface currents (i.e., upper ADCP bins) averaged 1 h before the arrivals and across BDB and SHB. Then, c is estimated for all events propagating between SHB and BDB by subtracting u_a. Figure 10b shows the linear regression between c and ΔT, which accounts for more than 50% of the variance in the data. From this analysis, $\bar{u}_a$ is 0.117 m s^{-1} agreeing with other order of 0.1 m s^{-1} estimates [e.g., *Drake et al.*, 2005]. A regression between c_{obs} (after removal of wind and tide components) and $c_p \approx c_w$ where c_w, is the propagation speed in the steep bottom slope limit as calculated from Table 2 suggest that this buoyant flow is surface-trapped under most conditions ($R^2 = 0.496$, $N = 37$, $p < 0.001$). The ratio of c_w to c_α, the propagation speed in the limit of a small bottom slope, also is much less than 1 supporting surface-trapped

Figure 8. Photo of convergent front offshore near the BDB line on 14 June 2007 at 0815 LT. Winds were light and front was propagating poleward.
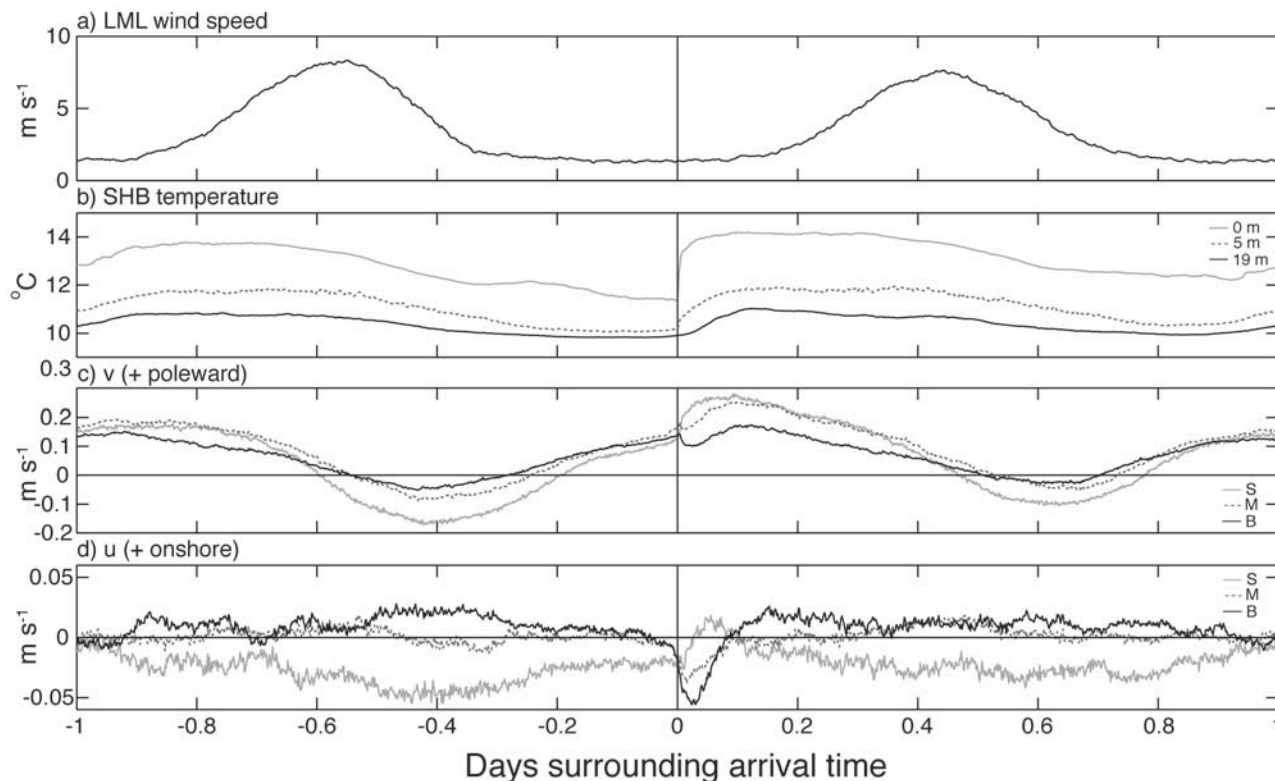
Figure 9. Composite average of front crossings from SHB20. (a) Local alongshore winds at LML (positive poleward), (b) temperatures at 3 depths (0, 5, 19 m) from SHB20, (c) alongshore (*v*) current velocities, and (d) cross-shore (*u*) current velocities at 3 depths (surface, midwater, and bottom) from SHB20.

buoyant flow (Table 2) [*Lentz and Helfrich*, 2002]. Again, the offset agrees with the order of 0.10 m s^{-1} estimates of the subinertial alongshore currents in the region [*Drake et al.*, 2005]. We further compared c and the near-surface current speed just after frontal arrival, c_f (averaged over ~1 h at BDB and SHB with values being averaged together). The convergence shown in Figure 9c and $c_f > c$ indicate supercritical flow during poleward frontal propagation.

[27] To evaluate our estimates of propagation speeds, we conducted a momentum balance using equation 4 and calculated the alongshore wind required to create an opposing alongshore current equal to the propagation speed of the front (4.9 m s^{-1}). In addition, alongshore, wind-driven currents, $v_w = \tau^{sy}/\rho_0^r$ (drag coefficient, $r = 5 \times 10^{-4}$ m s^{-1}), were estimated assuming a balance between surface and bottom stress. When wind driven currents are greater than c, the front will move equatorward and back into the bay. On the basis of this analysis, wind speeds greater than approximately 6.2 m s^{-1} caused the front to move south and into the bay. Values of wind speeds that lead to equatorward frontal movement from both methods (momentum balance and propagation speed) agree reasonably well (4.9 and 6.2 m s^{-1}, respectively).

[28] Positive (northward, westward) velocities combined with warm surface water temperature are indicative of a site being situated within the upwelling shadow, negative velocities (southward, eastward) and cold surface temperatures are indicative of the site being within the upwelling

plume. Zero crossings in the surface current data with concurrent increases in temperature indicate when the front crossed a site. Using these criteria, BDB and SHB were located within the upwelling shadow roughly 33% and 66% of the study period, respectively, and were frequently crossed by the upwelling shadow front (Table 2). Conversely, TPT and LHP were consistently within the upwelling shadow when it was present.

[29] Figure 11a shows the regional wind time series from NDBC buoy 46042 during the study period along with the location of the front alongshore in Figure 11b. The LHP mooring array was used as the origin with positive values indicating frontal positions poleward of LHP and negative values indicating positions equatorward of LHP. The front moved rapidly to the northwest directly after the relaxation of regional upwelling favorable winds (for example, relaxation event 5 in Figure 11). The front moves poleward within a few hours of wind relaxation as the upwelling shadow moves out of the bay and is replaced by cool waters of the upwelling plume during longer relaxation events. The upwelling shadow is not present within the study area during longer relaxation events (Figures 11b and 11d). The 11°C isotherm moves equatorward during afternoons as equatorward wind-driven currents strengthen. In the afternoon, strong diurnal upwelling winds often cause the front to separate from the coast as warm water moves offshore and is replaced by cooler water nearshore. The warm water mass appears to move back onshore as upwelling winds relax. This process has previously been described

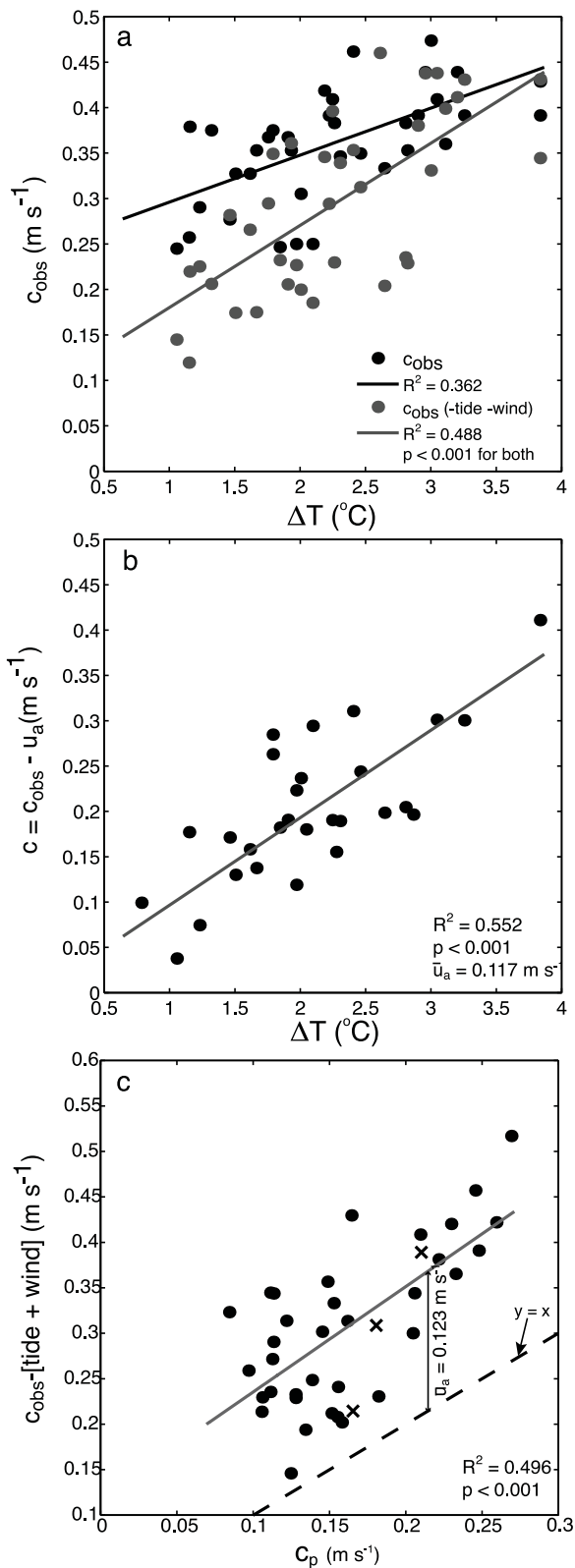as local diurnal upwelling for this region [*Woodson et al.*, 2007].
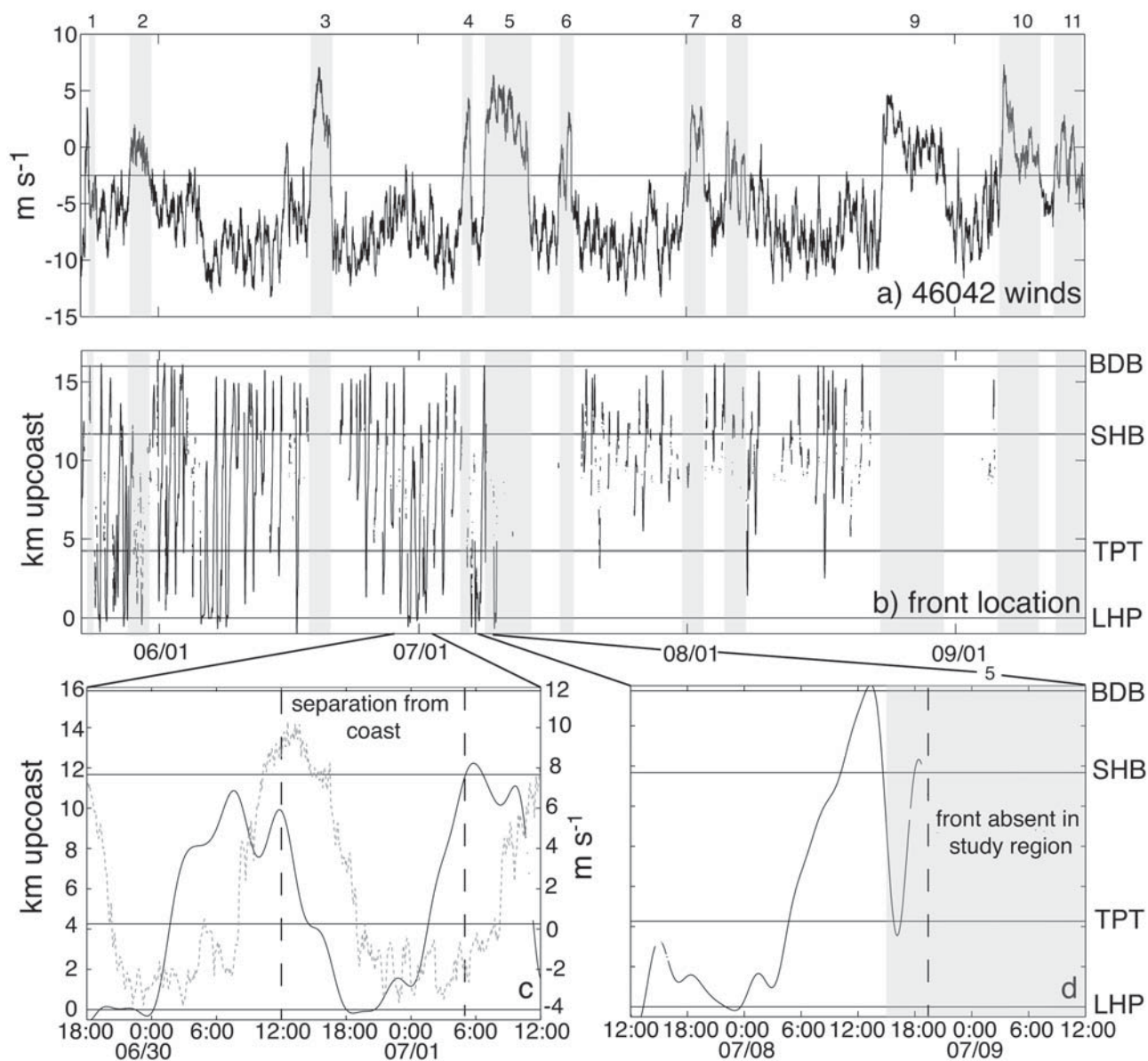
4. Discussion

[30] The results of this study demonstrate that the location of the upwelling shadow front between recently upwelled waters and the upwelling shadow in northern Monterey Bay is determined by the modification of the regional oceanographic conditions (the upwelling shadow) by local forcing conditions. The presence and location of the upwelling shadow front is typically determined by a balance among several factors. These are diurnal upwelling winds, buoyancy forcing due to temperature differences between upwelled waters and the upwelling shadow, and what we hypothesize is a poleward barotropic pressure gradient resulting from sea level differences between Monterey Bay and Point Año Nuevo. When local winds are weak at night and in the early morning, the upwelling front moves poleward alongshore due to buoyancy forcing and the barotropic pressure gradient. Equatorward winds strengthen during the late morning and early afternoon to produce equatorward alongshore currents, which then advect the upwelling shadow front into the bay. The upwelling shadow front can move up and down the coast up to 5 km in a day. However, this daily movement is more frequently restricted to less than 4 km since the front often did not cross two sites in the same day, and if so, only SHB and BDB. Extended wind relaxations lead to the upwelling shadow front propagating poleward and out of the study area. The observed poleward velocities below and just ahead of the upwelling shadow (e.g., Figure 9) are consistent with our hypothesis of a barotropic pressure gradient that develops due to intense upwelling to the north of the bay and higher sea level in the bay. The sea level difference in this case leads to upcoast flow in the absence of a density gradient [*Gan and Allen*, 2005].

[31] Scaling parameters and definitions for buoyancy-driven currents in frontal equilibrium are given in Table 3 [after *Lentz and Helfrich*, 2002]. To isolate the buoyancy-driven component of the flow for calculation of frontal propagation speeds, physical data were taken from early morning hours when winds had been calm for >8 h. This period allowed for the buoyancy current to begin to move upcoast and was sufficiently long to reach frontal equilibrium (e.g., greater than $t_{adj} = 0.897$ h, and $f^{-1} = 3.18$ h) although we suspect that the front does not fully achieve geostrophic balance.

[32] The ratio of the propagation speeds, c_w/c_α, is the important scaling factor under upwelling favorable conditions. Using the observed values of current depth and temperature difference across the front, c_w/c_α is consistently on the order of 0.1. These values of c_w/c_α reported here are comparable to observations of *Lentz and Largier* [2006],

Figure 10. Scatterplot of (a) c_{obs} versus ΔT showing both raw c_{obs} and c_{obs} with wind and tide constituents removed, (b) $c = c_{obs} - u_a$ versus ΔT, and (c) c_{obs} (wind and tidal components removed) versus c_p for 37 front crossing observations (solid circles) during calm wind conditions (<3 m s^{-1}) and 3 front crossings during regional relaxation events (cross). Offset of linear regression is 0.1057 m s^{-1} agrees well with observed geostrophic northward flow at SHB [*Drake et al.*, 2005]. Diurnal and semidiurnal tidal components of c_{obs} removed using T_TIDE. Local wind driven current component of c_{obs} removed using correction from *Lentz and Largier* [2006].

Figure 11. Time series of (a) regional along-shelf wind speed measured at NDBC46042 (positive is northwestward) and (b) location along coast of the 11°C isotherm as a proxy for frontal location (see section 2). (c) Same as in Figure 11b, over shorter period during regional upwelling, local winds (LML) are shown with gray dashed line and (d) same as in Figure 11b over shorter period during a transition from regional upwelling to relaxation. Grey in Figures 11b–11d indicate location of cross-shelf mooring arrays. Grey shading indicates regional wind relaxation periods.

when accounting for the reduced buoyancy difference and the increase in the bottom slope by a factor of approximately 10 in northern Monterey Bay in comparison with the North Carolina shelf. Thus, the upwelling shadow current behaves as a surface-trapped buoyancy current during light upwelling favorable winds. Stronger upwelling favorable winds in the afternoon cause the front to be arrested, move back into the bay, and potentially separate from the coast [e.g., *Lentz and Largier*, 2006; *Woodson et al.*, 2007].

[33] Temperature differences explain ~50% of the variance in c_{obs} suggesting that front propagation is significantly buoyancy driven. Agreement with scaling theory suggest that the water mass behaves as a surface-trapped buoyant plume, although geostrophic balance is not likely for the

diurnal movements observed in this study. The offset of 0.124 m s^{-1} in Figure 10b is consistent with the ~0.10 m s^{-1} northward geostrophic flow in the region as estimated from scaling theory and long-term observations [e.g., *Drake et al.*, 2005] and suggests that the front propagation is riding on a mean northward geostrophic flow.

[34] In other buoyant coastal currents, such as the outflow of the Chesapeake Bay, wind stress has been observed to modulate frontal advection speed [*Lentz and Largier*, 2006]. We observed a significant effect of wind-induced surface currents. When winds increased during the day, the front was observed to move back into the bay. We estimated the wind strength necessary to initiate equatorward movement of the front is approximately 5 m s^{-1}. This value leads to a
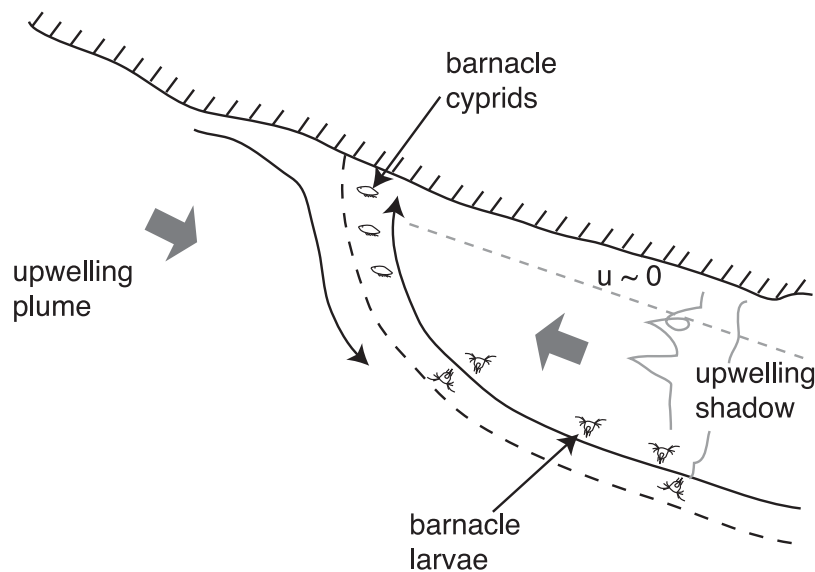
Figure 12. Illustration of frontal circulation for a surface trapped buoyancy current following *Lentz and Helfrich* [2002] during upwelling season. Grey arrows show direction of residual currents with longer arrows representing stronger currents closer to the front location.

ratio of $c_w/c_\alpha \sim 1$. As winds increased further, the front separated from the coast leading to diurnal upwelling [*Woodson et al.*, 2007].

[35] Fronts are often regions with sharply increased primary production and higher trophic level activity [*Traganza et al.*, 1987; *Healey et al.*, 1990; *Graham*, 1993]. Onshore translation of offshore fronts generated by regional-scale upwelling is believed to lead to recruitment pulses of many marine species ranging from barnacles to rockfish [*Roughgarden et al.*, 1991; *Bjorkstedt et al.*, 2002]. Retention zones behind headlands are also known to show increased larval abundances and recruitment of many species [*Wing et al.*, 1995]. However, the resulting impacts of nearshore fronts such as the one described in this study on biological factors such as settlement and community structure are not well understood. Our results suggest that only relaxation events lasting 5 days or more allow offshore upwelling fronts to reach coastal habitats in the northern Monterey Bay region. However, coastally trapped water masses such as the northern Monterey Bay upwelling shadow and its associated front move up the coast with little or no lag (less than 3 h) in response to changes in the regional-scale wind regime.

[36] We further hypothesize that circulation within the upwelling shadow near the front provides a mechanism for very nearshore retention and transport of larvae and passive particles to the coast (Figure 12). On the basis of 37 observed circulation patterns within the front reported in this study and in laboratory studies of surface-trapped buoyancy flows (Figure 8) [*Lentz and Helfrich*, 2002], currents and material within the upwelling shadow travel first offshore, then along the front, and eventually toward the coast near the nose of the front. Larvae that reside just inside the front will thus be advected toward the shore. Cross-shore currents are directed offshore most of the time at speeds (10^{-2} m s^{-1}) greater than the swimming capabilities of many nearshore invertebrate larvae (10^{-4} m s^{-1}). Consequently, transport to shore requires either that larvae

aggregate deeper in the water column or near the convergent front. These observations further suggest that alongshore movements of nearshore fronts may drive recruitment patterns for nearshore and intertidal species in regions dominated by alternating headlands and bays such as within the CCLME.

[37] In addition, higher observed chlorophyll concentrations at nearshore fronts and clines (in this study, the front is the surface expression of the pycnocline that extends well into the bay) may increase larval food supply [*McManus et al.*, 2005; *Ryan et al.*, 2008a, 2008b], enhance recruitment and increase adult growth at sites where the front is more consistently located (e.g., SHB in our study). The occurrence of topographically driven, thermally modulated retention zones in the CCLME, such as reported here, may allow for increased recruitment and reduced dispersal of nearshore and intertidal organisms.

5. Conclusions

[38] Regional-scale winds and topography lead to the development of a warm water lens in the wind shadow of northern Monterey Bay [*Graham and Largier*, 1997]. A front then develops at the boundary between upwelled waters and the upwelling shadow within the bay. The upwelling shadow moves up and down the coast with a quasiperiodic motion due to interactions between an alongshore pressure gradient, caused by regional upwelling, local surface heating, and local wind forcing. The relative contributions of regional upwelling and local buoyancy forcing to the alongshore pressure gradient appear to be of the same order of magnitude.

[39] The upwelling shadow front is typically in contact with the shore and moves in an alongshore direction up to a 5 km each day and was consistently located within the focal point of our study area near Sand Hill Bluff. A balance between the pressure gradient (barotropic and baroclinic) and the local wind stress determines the location of the front

along the coast. Currents behind the upwelling shadow front are typically poleward in contrast to equatorward currents within recently upwelled waters. During regional-scale relaxation events, the warm upwelling shadow and associated front are advected northward along the coast resulting in initial warming of waters outside the front. Once upwelling favorable winds resume, waters in the shadow region quickly warm and create a new upwelling shadow water mass. The variability of the oceanographic response to regional- and local-scale forcing suggests that resulting patterns in biological characteristics such as recruitment and settlement of marine larvae are dependent on regional-scale forcing. However, such patterns may ultimately be driven by local-scale processes to the extent that local conditions may alter or even reverse the expected patterns due to regional-scale observations. The three-dimensional frontal dynamics reported in this study provide a distinct mechanism for the transport of larvae to shore by breaking the two-dimensional cross-shelf wind-driven circulation. The consequent responses of biological systems in such regions also require further investigation.

References

Banta, R. M., L. D. Oliver, and D. H. Levinson (1993), Evolution of the Monterey Bay sea-breeze layer as observed by pulsed Doppler LIDAR, *J. Atmos. Sci.*, 50, 3959–3982, doi:10.1175/1520-0469(1993)050<3959:EOTMBS>2.0.CO;2.

Beardsley, R. C., C. Dorman, C. Friehe, L. Rosenfeld, and C. Winant (1987), Local atmospheric forcing during the Coastal Ocean Dynamics Experiments 1 and 2: 1. A description of the marine boundary layer and atmospheric conditions over a northern California upwelling region, *J. Geophys. Res.*, 92, 1467–1488, doi:10.1029/JC092iC02p01467.

Beardsley, R. C., E. P. Dever, S. J. Lentz, and J. P. Dean (1998), Surface heat flux variability over the northern California shelf, *J. Geophys. Res.*, 103, 21,553–21,586, doi:10.1029/98JC01458.

Bjorkstedt, E. P., L. K. Rosenfeld, B. A. Grantham, Y. Shkedy, and J. Roughgarden (2002), Distributions of larval rockfishes Sebastes spp. across nearshore fronts in a coastal upwelling region, *Mar. Ecol. Prog. Ser.*, 242, 215–228, doi:10.3354/meps242215.

Breaker, L. C., and W. W. Broenkow (1994), The circulation of Monterey Bay and related processes, *Oceanogr. Mar. Biol.*, 32, 1–64.

Drake, P. T., M. A. McManus, and C. D. Storlazzi (2005), Local wind forcing of the Monterey Bay area inner shelf, *Cont. Shelf Res.*, 25, 397–417, doi:10.1016/j.csr.2004.10.006.

Franks, P. J. S. (1995), Thin layers of phytoplankton: A model of formation by near-inertial wave shear, *Deep Sea Res., Part I*, 42, 75–91, doi:10.1016/0967-0637(94)00028-Q.

Gan, J. P., and J. S. Allen (2005), Modeling upwelling circulation off the Oregon coast, *J. Geophys. Res.*, 110, C10S07, doi:10.1029/2004JC002692.

Graham, W. M. (1993), Spatio-temporal scale assessment of an "upwelling shadow" in northern Monterey bay, California, *Estuaries*, 16, 83–91, doi:10.2307/1352766.

Graham, W. M., and J. L. Largier (1997), Upwelling shadows as nearshore retention sites: The example of northern Monterey Bay, *Cont. Shelf Res.*, 17, 509–532, doi:10.1016/S0278-4343(96)00045-3.

Healey, M. C., R. E. Thomson, and J. F. T. Morris (1990), Distribution of commercial troll fishing vessels off southwest Vancouver Island in relation to fishing success and oceanic water properties and circulation, *Can. J. Fish. Aquat. Sci.*, 47, 1846–1864, doi:10.1139/f90-210.

Hickey, B. M. (1979), The California current system–Hypotheses and facts, *Prog. Oceanogr.*, 8, 191–279.

Kirincich, A. R., J. A. Barth, B. A. Grantham, B. A. Menge, and J. Lubchenco (2005), Wind-driven inner-shelf circulation off central Oregon during summer, *J. Geophys. Res.*, 110, C10S03, doi:10.1029/2004JC002611.

Large, W. G., and S. Pond (1981), Open ocean momentum flux measurements in moderate to strong winds, *J. Phys. Oceanogr.*, 11, 324–336, doi:10.1175/1520-0485(1981)011<0324:OOMFMI>2.0.CO;2.

Lentz, S. J., and K. R. Helfrich (2002), Buoyant gravity currents along a sloping bottom in a rotating fluid, *J. Fluid Mech.*, 464, 251–278, doi:10.1017/S0022112002008868.

Lentz, S. J., and J. Largier (2006), The influence of wind forcing on the Chesapeake Bay buoyant coastal current, *J. Phys. Oceanogr.*, 36, 1305–1316, doi:10.1175/JPO2909.1.

McManus, M. A., O. M. Cheriton, P. J. Drake, D. V. Holliday, C. D. Storlazzi, P. L. Donaghay, and C. F. Greenlaw (2005), Effects of physical processes on structure and transport of thin zooplankton layers in the coastal ocean, *Mar. Ecol. Prog. Ser.*, 301, 199–215, doi:10.3354/meps301199.

Mooers, C. N. K. (1968), A compilation of observations from moored current meters and thermographs, in *Volume 2: Oregon Continental Shelf, August–September 1966, Data Rep. 68-5*, Oreg. State Univ., Corvallis.

Pawlowicz, R., B. Beardsley, and S. Lentz (2002), Classical tidal harmonic analysis including error estimates in MATLAB using T_TIDE, *Comput. Geosci.*, 28, 929–937, doi:10.1016/S0098-3004(02)00013-4.

Pennington, J. T., and F. P. Chavez (2000), Seasonal fluctuations of temperature, salinity, nitrate, chlorophyll and primary production at station H3/M1 over 1989–1996 in Monterey Bay, California, *Deep Sea Res., Part II*, 47, 947–973, doi:10.1016/S0967-0645(99)00132-0.

Pineda, J. (1999), Circulation and larval distribution in internal tidal bore warm fronts, *Limnol. Oceanogr.*, 44, 1400–1414.

Rosenfeld, L. K., F. B. Schwing, N. Garfield, and D. E. Tracy (1994), Bifurcated flow from an upwelling center: A cold water source for Monterey Bay, *Cont. Shelf Res.*, 14, 931–964, doi:10.1016/0278-4343(94)90058-2.

Roughgarden, J., J. T. Pennington, D. Stoner, S. Alexander, and K. Miller (1991), Collisions of upwelling fronts with the intertidal zone: The cause of recruitment pulses in barnacle populations of central California, *Acta Oecol.*, 12, 35–51.

Ryan, J. P., M. A. McManus, J. D. Paduan, and F. P. Chavez (2008a), Phytoplankton thin layers caused by shear in frontal zones of a coastal upwelling system, *Mar. Ecol. Prog. Ser.*, 354, 21–34, doi:10.3354/meps07222.

Ryan, J. P., J. F. R. Gower, S. A. King, W. P. Bissett, A. M. Fischer, R. M. Kudela, Z. Kolber, F. Mazzillo, E. V. Rienecker, and F. P. Chavez (2008b), A coastal ocean extreme bloom incubator, *Geophys. Res. Lett.*, 35, L12602, doi:10.1029/2008GL034081.

Shanks, A. L., and L. Brink (2005), Upwelling, downwelling, and cross-shelf transport of bivalve larvae: Test of a hypothesis, *Mar. Ecol. Prog. Ser.*, 302, 1–12, doi:10.3354/meps302001.

Storlazzi, C. D., M. A. McManus, and J. D. Figurski (2003), Long-term, high-frequency current and temperature measurements along central California: Insights into upwelling/relaxation and internal waves on the inner shelf, *Cont. Shelf Res.*, 23, 901–918, doi:10.1016/S0278-4343(03)00045-1.

Traganza, E. D., D. G. Redalje, and R. W. Garwood (1987), Chemical flux, mixed layer entrainment, and phytoplankton blooms at upwelling fronts in the California coastal zone, *Cont. Shelf Res.*, 7, 89–105, doi:10.1016/0278-4343(87)90066-5.

Wing, S. R., L. W. Botsford, J. L. Largier, and S. E. Morgan (1995), Spatial structure of relaxation events and crab settlement in the northern California upwelling system, *Mar. Ecol. Prog. Ser.*, 128, 199–211, doi:10.3354/meps128199.

Woodson, C. B., and M. A. McManus (2007), Foraging behavior can influence dispersal of marine organisms, *Limnol. Oceanogr.*, 52, 2701–2709.

Woodson, C. B., et al. (2007), Diurnal upwelling driven by sea breezes in northern Monterey Bay, *Cont. Shelf Res.*, 27, 2289–2302, doi:10.1016/j.csr.2007.05.014.

———————

J. A. Barth, College of Oceanic and Atmospheric Sciences, Oregon State University, Corvallis, OR 97331, USA.

D. J. Hoover, United States Geological Survey, 400 Natural Bridges Dr., Santa Cruz, CA 95060-5792, USA.

A. R. Kirincich, Physical Oceanography, Woods Holes Oceanographic Institute, 266 Woods Hole Rd. MS #21, Woods Hole, MA 02543, USA.

M. A. McManus, Department of Oceanography, University of Hawai'i at Mānoa, Marine Science Building, 1000 Pope Rd., Honolulu, HI 96822, USA.

J. P. Ryan, Research and Development, Monterey Bay Aquarium Research Institute, P.O. Box 628, Moss Landing, CA 95039, USA.

J. Tyburczy, Department of Zoology, Oregon State University, 3029 Cordley Hall, Corvallis, OR 97331, USA.

L. Washburn, Geography Department, University of California, Santa Barbara, Santa Barbara, CA 93106, USA.

C. B. Woodson, Environmental Fluid Mechanics Lab, Stanford University, Stanford, CA 94305, USA. (bwoodson@stanford.edu)